Heterojunction PbS Nanocrystal Solar Cells with Oxide Charge-Transport Layers

Byung-Ryool Hyun,[†,*] Joshua J. Choi,[‡] Kyle L. Seyler,[†] Tobias Hanrath,[‡] and Frank W. Wise[†]

[†]School of Applied and Engineering Physics and [‡]School of Chemical and Biomolecular Engineering, Cornell University, Ithaca, New York 14853, United States

ABSTRACT Oxides are commonly employed as electron-transport layers in optoelectronic devices based on semiconductor nanocrystals, but are relatively rare as hole-transport layers. We report studies of NiO hole-transport layers in PbS nanocrystal photovoltaic structures. Transient fluorescence experiments are used to verify the relevant energy levels for hole transfer. On the basis of these results, planar heterojunction devices with ZnO as the photoanode and NiO as the photocathode were fabricated and characterized. Solution-processed devices were used to systematically study the dependence on nanocrystal size and achieve conversion efficiency as high as 2.5%. Optical modeling indicates that optimum performance should be obtained with thinner oxide layers than can be produced reliably by solution casting. Room-temperature sputtering allows deposition of oxide layers as thin as 10 nm, which enables optimization of device performance with respect to the thickness of the charge-transport layers. The best devices achieve an open-circuit voltage of 0.72 V and efficiency of 5.3% while eliminating most organic material from the structure and being compatible with tandem structures.

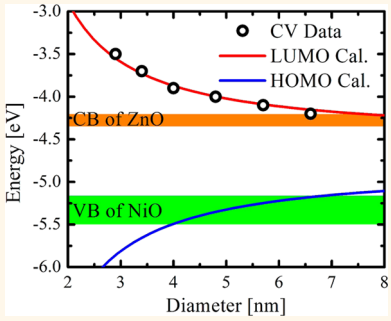

KEYWORDS: excitonic solar cells · heterojunction solar cells · ZnO photoanode · NiO photocathode · PbS nanocrystals · hole transfer · electron transfer · inverted solar cells

Nanocrystal (NC) heterojunction photovoltaic structures that can be fabricated by simple processing techniques are under intense investigation because of their potential for efficient and low-cost devices.[1−3] It is therefore important to identify suitable combinations of materials from which such heterojunctions can be formed and to understand the mechanisms behind their operation, which is complicated by difficulties in establishing accurate electron affinities and ionization potentials of materials. In heterojunction solar cells, interfacial layers suppress contact resistance between the active layer and charge-collecting electrodes,[1] create ohmic contacts, and efficiently transport charges,[4] all of which improve the power conversion efficiency of solar cells without interfacial layers. Electron and hole blocking can improve the operating voltage, and rapid dissociation of photogenerated excitons increases photocurrent. In addition, when the active layer is sandwiched between two electrodes, the incident light forms a standing wave inside the active layer.[5,6] The optical intensity can be distributed maximally within the NC film by using dielectric contrast and efficiently blocking minority carriers.[7]

Various buffer layer materials have been used at the NC active layer/electrode interface to improve cell performance. Among them, zinc oxide (ZnO)[1,2,8] and titanium dioxide (TiO_2)[4,9] have been used for electron-transport (hole blocking), whereas several metal oxides such as molybdenum oxide (MoO_3),[10−12] vanadium oxide (V_2O_5),[11,12] and tungsten oxide (WO_3)[13] have been used for the hole-transport (electron-blocking) layer. The use of ZnO and TiO_2 for extracting electrons from NCs is obvious because they are n-type materials. However, the rationale for the selection of the hole-transport layer is unclear because MoO_3, V_2O_5, and WO_3 are also n-type. Thus, the physical mechanism behind the enhancement of efficiency of solar cells with those layers, including the interface selectivity,[14] is still in debate, although it has been attributed to more favorable energy level alignment.[7,11,15]

* Address correspondence to bh73@cornell.edu.

Received for review August 26, 2013 and accepted November 25, 2013.

Published online November 25, 2013
10.1021/nn404457c

Dye-sensitized solar cells,[16−19] organic solar cells,[19−25] and NC light emitting diodes (LEDs)[26−28] based on nickel oxide (NiO) have been reported and show that NiO can be used as an efficient hole-transport layer. NiO is a p-type semiconductor with an optical energy gap of 4 eV[29−31] and a transport gap of 4.3 eV.[32] The ionization potential (IP) of NiO is the smallest among p-type metal oxides, even allowing for variation in the literature from 5.16 (ref 33) to 5.4 (ref 27) and 5.5 (ref 34) eV. The electron affinity (EA) of NiO is reported to be 1.4−1.6 eV.[27,35,36] This small value should enable hole transfer from most NCs, including Pb salt NCs, to NiO. Furthermore, the hole mobility of NiO is between 20 and 50 $cm^2 \cdot V^{-1} \cdot s^{-1}$ at room temperature,[37] which is high for p-type metal oxides. Thus, NiO could be an excellent choice for the hole-transport layer in solar cells. However, up to now, the use of NiO layers in NC solar cells has not been reported.

Previous work has shown that the photovoltage of NC solar cells is proportional to the NC energy gap,[1,38] and Nair *et al.* argue that the primary benefit of quantum confinement will be to increase the photovoltage of the cell.[39] Ma *et al.* reported a study of PbSe NCs with diameter as small as 1 nm.[40] These workers found that the open-circuit voltage decreases for diameters below 2 nm, which produced an open-circuit voltage of 0.6 eV. A similar value was obtained by use of a shallow-work-function electrode.[41] Very recently, improved passivation of the NC surfaces allowed an open-circuit voltage of 0.69 V to be achieved.[42]

Here, we describe heterojunction PbS NC solar cells with ZnO photoanodes and NiO photocathodes produced by simple processing techniques. We first present results on photoinduced hole transfer from NCs to NiO. With this process as the basis of the devices, we construct prototype solar cells by low-temperature solution processing. These devices achieve reasonable performance, including a power conversion efficiency of 2.5%. Optimization of the device performance requires greater control of layer thickness, which we achieve by room-temperature sputtering of the oxide layers. The resulting devices exhibit an efficiency above 5% and the largest open-circuit voltage (0.72 V) reported for single-junction NC solar cells to our knowledge. In addition to promising performance, these devices are a step toward all-inorganic structures that are directly compatible with future tandem cells.[16,17] Here we focus on the demonstration of PbS NC solar cells with NiO photocathodes. A side-by-side comparison study of cells produced by solution processing and sputtering will be the subject of future work, along with the optimal cell design for maximum efficiency.

The relevant energy levels of a heterojunction ZnO/PbS NC/NiO solar cell are shown in Figure 1. The EA of n-type ZnO is between 4.2 (refs 19, 43, 44) and 4.35 (ref 45) eV. The EAs for PbS NCs with various sizes were measured by cyclic voltammetry (CV), and the relevant energy levels were calculated by using a four-band model based on a $k \cdot p$ Hamiltonian incorporating quantum confinement of charge carriers together with dielectric effects.[46]

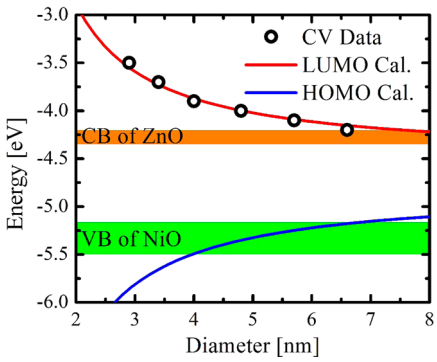

Figure 1. Energy levels of ZnO/PbS NC/NiO thin films. Values for the conduction band (CB) of n-type ZnO range from 4.2 to 4.35 eV (orange block), and the valence band (VB) of p-type NiO ranges from 5.16 to 5.5 eV (green block). Symbols are measured values for PbS NCs, and lines are calculated energy levels.

The comparison of PbS NC and ZnO energy levels indicates that electron transfer from PbS NCs to ZnO is favorable for PbS NCs with diameters less than ~7 nm. Electron extraction from PbS NCs to ZnO in PbS NC/ZnO heterojunctions[1,2,47] and PbS NC-sensitized solar cells[48] is well established in the literature. Owing to the low IP value of NiO, hole transfer from PbS NCs to NiO is thermodynamically favorable for PbS NCs with diameters less than ~5 nm. However, there is no experimental study of hole transfer from PbS NCs to NiO. To verify the hole transfer from PbS NC, fluorescence quenching measurements were performed with PbS NCs coupled to NiO.

Direct chemical coupling of PbS NCs to a NiO mesoporous film with linker molecules with carboxylic acid or other functional groups is difficult in our experience. This is perhaps surprising, given that dye molecules with such groups have been used in NiO-based dye-sensitized solar cells. We circumvented this problem by first attaching PbS NCs to mesoporous SiO_2 film as an inert base platform and then attaching NiO particles to PbS NCs. The EA of SiO_2 is reported to be 0.9 eV[49] or 1.0 eV,[50] and its energy gap is 8.9 eV.[51] Thus, we expect no charge transfer between PbS NCs and SiO_2. This is supported by results with the CdSe NC−SiO_2 system;[52] CdSe NCs have a lower EA than PbS NCs. Furthermore, electron transfer between PbS NCs and linker molecules with carbon chains and the thiol group can be ruled out because of the energy level alignment.[46] PbS NCs were first coupled to mesoporous SiO_2 film with mercaptocarboxylic acid; then oleic acid ligands on the surface of PbS NCs were removed with 2-mercaptoethanol (MEtOH). Finally,

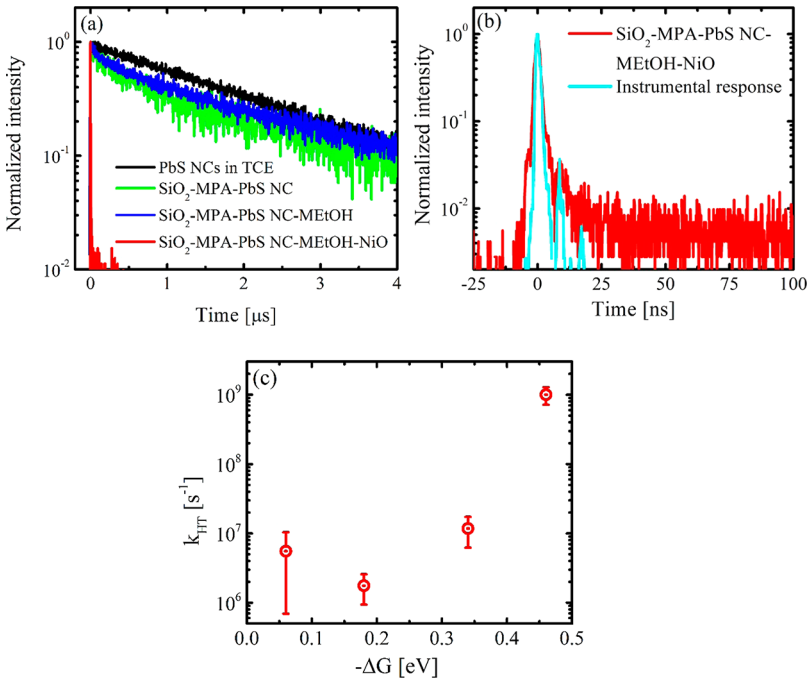

Figure 2. (a) Transient fluorescence traces of 3.5 nm PbS NCs in TCE (solid black line), SiO_2—MPA—PbS NC composites (solid green line), SiO_2—MPA—PbS NC—MEtOH composites (solid blue line), and SiO_2—MPA—PbS NC—MEtOH—NiO composites (solid red line). (b) Transient fluorescence of 3.5 nm PbS NCs coupled to NiO nanoparticles, along with the instrument response. (c) Dependence of hole transfer constant, k_{HT}, on the change in free energy for the PbS NC—NiO system.

the NiO nanoparticles were coupled to PbS NCs by physical contact. Details are in the Methods or Supporting Information.

RESULTS AND DISCUSSION

Fluorescence transients were measured for PbS NCs of diameter 3.5, 4, 5, and 6 nm. The spectral range of our photodetector (950—1700 nm) precludes the investigation of larger NCs. The fluorescence of the 3.5 nm PbS NCs in tetrachloroethylene (TCE) decays with a time constant of 1.7 μs (black line in Figure 2a). The decay times for control samples of SiO_2—PbS NC (green line) and SiO_2—PbS NC—MEtOH (orange line) systems are 0.8 and 1.1 μs, respectively. While the energy level alignment does not allow charge transfer between PbS NCs and SiO_2, we conjecture that the slightly faster recombination for the PbS NC—SiO_2 system derives from a combination of aggregation of PbS NCs on the surface of the SiO_2 and changes in the NC surface chemistry.[53] In contrast, the NC fluorescence is quenched dramatically in the presence of the NiO (Figure 2b); the fluorescence decay is close to the ~1 ns instrument response. For the larger NCs, quenching is also observed, but it is much slower (Figure S2 in the Supporting Information). The decay maintains a microsecond-scale time component in addition to the nanosecond component.

The time for the population to decay to 10% of the initial photoexcited value, for example, does not increase monotonically with NC size, which would be expected in a Marcus-theory view of the charge transfer. If we assume that the observed decrease in lifetime arises from hole transfer into NiO, the hole transfer rate constant can be determined through the expression[46,54] $k_{HT} = 1/\tau_{NC-NiO} - 1/\tau_{NC}$, where τ_{NC-NiO} and τ_{NC} are 1/e decay times of the PbS NC—NiO system and PbS NCs, respectively. Our previous work[46] showed that the fluorescence decays of isolated NCs and NC—TiO_2 are the same if the LUMO level of the NCs is lower than the conduction band of TiO_2. The LUMO of the PbS NCs is well below the conduction band of SiO_2. This leads us to conclude that the PbS NC—SiO_2 system should have the same fluorescence decay as the isolated PbS NCs. Thus, we used the 1/e times the PbS NCs in TCE for calculating the hole-transfer rate. In Marcus theory,[55,56] the logarithm of the charge-transfer rate is a quadratic function of the change in free energy. In the present experiments, this is determined by the energy difference between the highest occupied molecular orbital (HOMO) energies of PbS NCs and the valence band of NiO (taken to be 5.16 eV). The dependence of the hole-transfer rate on the change in free energy (inferred from Figure 1) is summarized in Figure 2c. The rate generally increases with the free-energy difference, as expected within Marcus theory, although there is a reproducible deviation from the trend for the largest NCs. The results also suggest that the IP of NiO may be smaller than 5.2 eV, which is consistent with the value from X-ray photoelectron spectroscopy.[33]

Results from optical studies detailed above motivate the study of NiO films as the photocathode in NC thin

film solar cells. First, we fabricated heterojunction solar cells by sequential spin-coating of NiO sol–gel, a solution of PbS NCs, and ZnO nanoparticles on ITO substrates (Figure 3a). Detailed procedures are in the Methods section. Briefly, the NiO sol–gel precursor was prepared by dissolving nickel acetate tetrahydrate in methanol,[27] and colloidal ZnO nanoparticles were prepared from zinc acetate dihydrate in ethanol.[57,58] The NC films were treated with ethanedithol (EDT) to increase the film conductivity.[1,59,60] A high work function metal (Al, Au) was used as the back electron or hole-collecting electrode to reduce sensitivity to air. Device fabrication was performed under ambient conditions.

Figure 4a shows representative $J-V$ curves of solution-processed NiO/PbS NCs/ZnO devices for various diameters of PbS NCs. We observe a linear relation between V_{OC} and the size-dependent energy gap of PbS NCs consistent with prior reports on Schottky and excitonic lead salt NC solar cells.[1,38] A significant increase in the open-circuit voltage is observed with decreasing diameter of the NCs. A linear dependence of V_{OC} optical energy gap of the NCs is observed (Figure 4b).

The highest V_{OC} (0.68 V) is achieved for NCs with 2.8 nm PbS NCs ($E_g = 2$ eV) after 2 h of air exposure. This is very close to the highest value (0.69 V[42,61]) achieved by colloidal NC solar cells. We note that the air exposure leads to a substantial increase in both the V_{OC} and the fill factor (FF), and the photodoping induces a slight increase in photocurrent (data in the Supporting Information). Nitrogen exposure has no such positive effect, which suggests that the enhancement of the device performance is related to an oxygen-induced reaction in air. The best performance is obtained with 3 nm NCs, and a power conversion efficiency of 2.5% is achieved (Figure 5). With NC sizes for which hole transfer is marginally favorable or unfavorable energetically (greater than ~4 nm) we observe reverse-bias breakdown in the $J-V$ curves. The V_{OC} achieved with the NiO layers is slightly higher than the values[10,62–65] achieved with MoO_3 layers. However, we do not attach significance to the difference, as the comparison is not controlled.

The solution-processed devices have relatively high open-circuit voltage, and that of the best device is close to the highest reported for lead-chalcogenide NC solar cells.[40–42] However, the observed voltages are not close to fundamental limits. The 3 nm PbS NCs between ZnO and NiO contact layers experience similar energy level offsets for electron and hole extraction to the photoanode and photocathode, respectively. Nonradiative recombination reduces the photocurrent and the free charge concentration, which lowers the open-circuit voltage by decreasing the quasi-Fermi energy difference between electrons and holes. Strong suppression of nonradiative recombination is required to maximize the photocurrent.[66] The dark saturation current in solar cells mainly comes from the nonradiative recombination processes in the device, and thus dark saturation current can be considered a direct measure of the nonradiative recombination in the device. The optimized interfacial layer thickness is critical for reducing the dark saturation current by passivating localized traps in the NCs close to the junctions, and previous works have shown that layer thicknesses between 5 and 50 nm can lead to significant improvement in the performance of solar cells.[10–13,67]

We investigated the optimal thickness of the ZnO and NiO layers by optical modeling. Because of the dielectric contrast, reflections at interfaces affect the distribution of the optical field inside the solar cell structures. The generation of excitons depends on the distribution of the optical energy density, which consequently influences the photocurrent action spectra. This distribution can be optimized by controlling the

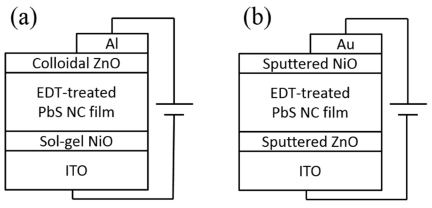

Figure 3. Device configuration of (a) solution-processed PbS NC solar cells and (b) inverted PbS NC solar cells with sputtered ZnO and NiO layers.

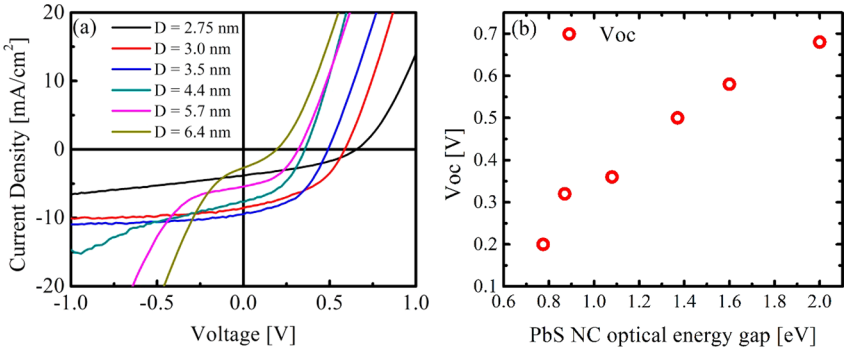

Figure 4. (a) Typical $J-V$ curves of ITO/NiO/PbS NC/ZnO/Al devices for various diameters of PbS NCs. (b) V_{OC} *versus* optical energy gap of PbS NCs.

thickness of the interfacial layers. We calculated the absorbance profile of the device stack as a function of NiO and ZnO layer thicknesses using a transfer matrix formalism[68−70] (Supporting Information). The structure glass/ITO/ZnO/PbS NCs/NiO/Au was used for the calculation of the optical modeling. As inputs to the calculations, the wavelength-dependent complex index of refraction of each layer in the device stack was measured using variable-angle spectroscopic ellipsometry. Results of the ellipsometry measurements are shown in Figure 6a.

The ellipsometry data were modeled with a set of Lorentz oscillators to obtain the complex index of refraction. The accuracy of the optical modeling was checked by comparing the calculated reflectance spectra from each thin film to the measured reflectance spectra using a spectrophotometer equipped with an integrating sphere. Calculations of the optical intensity in the device structure were performed assuming a fixed, 100 nm thickness of the EDT-treated PbS NC (1140 nm absorbance peak) layer and varying the ZnO and NiO thicknesses from 0 to 100 nm. The results show that the short-circuit current density is optimized near a NiO thickness of 25 nm, while thinner ZnO layers always produce higher current. In practice, the ZnO layer should be as thin as possible without sacrificing the integrity of the film. The peak at 25 nm for the NiO layer can be understood as an optical spacer effect: the placement of the active layer a few tens of nanometers away from the field-quenching metal electrode significantly increases the optical intensity in the active layer.[5,71]

The optical model suggests an optimal thickness of ZnO and NiO layers in the range of 5 to 40 nm to maximize the current density. However, deposition of high-quality layers with thickness below 30 nm is difficult *via* solution-based methods due to inherent surface roughness of such films. Furthermore, sol−gel NiO films require a high-temperature thermal treatment in air, which increases the resistivity of the ITO substrate. This naturally decreases the device performance[72] and will eventually be an impediment to tandem-cell development.

To overcome the limitations of solution-processed films, we deposited thin films of ZnO and NiO by room-temperature dc sputtering. This approach facilitates the fabrication of inverted solar cells, which have several advantages over the regular device structure seen in Figure 3a, such as improved stability and design flexibility for tandem or stacked cells. In the inverted device structure, ZnO and NiO layers are introduced above ITO or below the metal electrode as n-type and p-type interfacial layers as in Figure 3b. ITO is naturally n-type, so it is better suited to use as an electron acceptor, as is the case in the inverted structure.

The room-temperature sputtering conditions for depositing the crystalline ZnO and NiO layers were investigated based on the previous literature.[73] The detailed information for the sputtering conditions and physical characterizations of the sputtered films can be found in the Methods and Supporting Information.

The optical model suggests that greater than 60% increase in short-circuit current density can be obtained if the thickness of the oxide layers is tuned over the range 0−100 nm. We probed the relationship between film thickness and current density in devices based on EDT-treated active layers of 3 nm PbS NCs and 10 nm ZnO photocathodes. The open-circuit

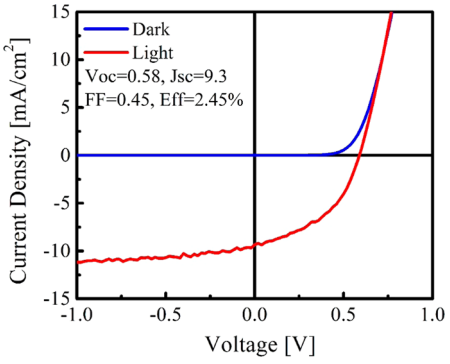

Figure 5. *J*−*V* curve of the best device prepared with sol−gel NiO, with 3 nm PbS NCs.

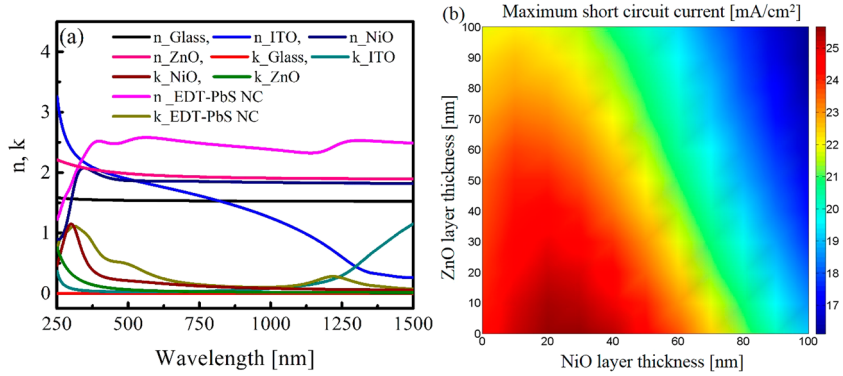

Figure 6. (a) Complex index of refraction of glass, ITO, NiO, and ZnO layers. (b) Current density calculated for varying thicknesses of ZnO and NiO layers.

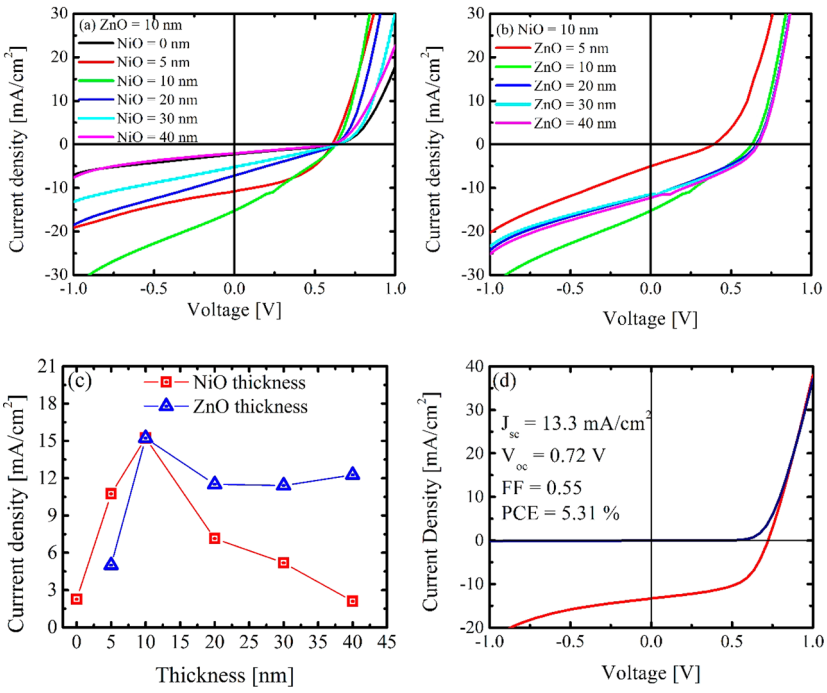

Figure 7. Typical *J*–*V* curves of the inverted PbS NC solar cells with the room-temperature-sputtered ZnO and NiO films. (a) The thickness of the ZnO layer was fixed at 10 nm, and the thickness of the NiO layer was varied from 0 to 40 nm. (b) The thickness of the NiO layer was fixed to 10 nm, and the thickness of the ZnO layer was varied from 5 to 40 nm. (c) Summary of current density with varying layer thickness. (d) Results from best device.

voltage is about 0.63 V for all devices (Figure 7a). However, the current density varies substantially. The current density exhibits a sharp maximum with respect to the thickness of the NiO (red squares in Figure 7c). On the other hand, when the thickness of the ZnO layer is varied with the thickness of the NiO layer fixed at 10 nm, the optimal thickness of ZnO is about 10 nm, but the difference of the current densities with 20 or 40 nm devices is relatively small (Figure 7c). Interestingly, the device with 5 nm ZnO shows a dramatic decrease in the current density. The best device has an open-circuit voltage of 0.72 V, short-circuit current of 13.3 mA/cm^2, and fill factor of 0.55, and achieves 5.3% efficiency. The open-circuit voltage is the largest reported for a NC solar cell to our knowledge.

The device structure based on a ZnO photoanode and a NiO photocathode deposited by room-temperature sputtering offers attractive features for NC tandem solar cells.[58,74] Metal oxide layers are commonly processed at high temperature to increase their crystallinity for better charge-carrier mobility.[75,76] High-temperature processing can present challenges in the fabrication of multijunction solar cells comprising temperature-sensitive NCs or organic active layers. Solution processing techniques generally lack the requisite precision in the fabrication of high-quality thin metal oxide films. The use of room-temperature-sputtered ZnO and NiO layers should enable fabrication of a simple series connection of photoanode/NCs/photocathode structures with accurately optimized layer thicknesses, which can give the sum of the maximum voltages of the component electrodes.[20]

CONCLUSION

In conclusion, we have synthesized and characterized NC solar cells with inorganic charge-transfer layers. Devices made with sol–gel NiO reach 2.5% efficiency. Sputtered films allow better control of film thickness, and room-temperature sputtering produces reasonably good films while avoiding thermal damage of the NCs. Optical modeling guided the determination of the optimum structure, which has 10 nm thick NiO and ZnO layers. Such devices exceed 5% efficiency and exhibit the highest open-circuit voltage reported for an NC solar cell. The approaches described here offer a route to efficient all-inorganic NC solar cells.

METHODS

PbS NC Synthesis and Purification. PbS NCs were synthesized based on a variation of a previous literature report.[77] Briefly, 20 mL of 1-octadecene (ODE) was added to a three-neck flask, which was vacuumed and purged with nitrogen gas three times to allow it to degas. The ODE was then heated to 110 °C, followed by two vacuum/purge cycles for 5 and 2 min to remove water and allow it to degas further. Afterward, the ODE was allowed to cool to room temperature in a nitrogen environment. Then 420 μL of bis(trimethylsilyl)sulfide (TMS) was added to the 20 mL of ODE and allowed to mix thoroughly. In

another three-neck flask, PbO, oleic acid, and ODE were mixed, degassed, and purged at 110 °C as before. Once the solution turned clear, indicating the formation of lead oleate, the flask temperature was lowered to a certain temperature. The mixture of TMS and ODE was then extracted and rapidly injected into the lead oleate solution using a syringe. After injection, the temperature dropped and the solution turned dark brown, indicating the formation of PbS NCs. The nanocrystal solution was left on the heating mantle for 3 min and, afterward, was cooled rapidly to room temperature with an ice bath. The nanocrystals were collected into centrifuge tubes, precipitated by adding twice the amount acetone as NC solution, and centrifuged for 5 min under ambient conditions. The supernatant was discarded and the NCs were redispersed in hexane. Acetone was once again added until the entire solution turned cloudy, and then the NCs were centrifuged, rinsed with acetone, and dried. The NCs were washed this way one more time for a total of three precipitations, and finally, they were redispersed at 40 mg/mL in chlorobenzene for solar cell fabrication and filtered through a 0.2 μm PVDF syringe filter to remove any dust, particulates, and NC aggregates.

PbS NC-Sensitized Mesoporous SiO_2 Films. Four grams of colloidal SiO_2 nanoparticles in water (Nalco 2327, diameter = 20 nm, 40 wt % aqueous dispersion) was diluted with 3.2 mL of water, and then, 0.64 g of polyethylene glycol (MW 20 000) was added into the diluted dispersion of SiO_2 nanoparticles. The mixture was stirred for at least 2 h. Thin films of SiO_2 nanoparticles were prepared on the glass substrate by using a spin-coating technique (1000 rpm, 30 s). Films were subjected to 450 °C heat treatment for 2 h. The temperature was then lowered to room temperature. Repeated steps of spin-coating and temperature treatment yielded the transparent mesoporous SiO_2 film of ~10 μm thicknesses. At the last thermal treatment, films were lowered to 120 °C. The hot films were placed directly in a 0.20 M 3-mercaptoacetic acid (MPA) (or 3-mercaptopropyl-trimethoxysilane, MPS) in toluene solution for 12 h. Films were washed three times with toluene and placed directly in PbS NCs in toluene for 24 h to sensitize PbS NCs. The PbS NC−SiO_2 films were washed three times with toluene to remove the unbound PbS NCs and then were dipped in a 1 M 2-mercaptoethanol in toluene solution to remove the oleic acid at the surface of the PbS NCs. The NiO nanoparticle solution was prepared by dispersing 1 g of NiO nanopowder (Inframat Advanced Materials, diameter = 20 nm) in 10 mL of water. After 0.5 h sonication, the NiO dispersion was left overnight to settle the big aggregations. The light brown supernatant was carefully pipetted. To add NiO nanoparticles inside the PbS NC−SiO_2 mesoporous film, a few 100 μL of NiO nanoparticles in water was dropped into the PbS NC−SiO_2 film and water was removed by an evaporation vacuum pump. This was repeated two or three times to fill the empty space inside the mesoporous film. The NiO nanoparticle-covered film was sealed by putting another cleaned glass slide on top and sealing the sides with UV-curable epoxy. Encapsulated samples were stable against oxidation for several months.

Fluorescence Lifetime Measurements. The samples were excited at a repetition rate of 1 kHz by femtosecond pulses of a Ti:sapphire laser system with an optical parametric amplifier (at 680 nm) or regenerative amplifier (at 800 nm). The sample was exposed to intensity levels below 10 mW/cm^2 so that the excitation level was always well below one electron−hole pair per dot. Fluorescence below 1000 nm was monitored with a Si avalanche photodiode single photon counting module (PerkinElmer, SPCM-AQRH-44-FC). The time-resolved fluorescence measurements were performed in the time-correlated single photon counting (TCSPC) mode with a TCSPC board (PicoQuant, TimeHarp 200) and a digital delay generator (Stanford Research Systems, DG645) under right-angle sample geometry. The fluorescence decay curves were analyzed by means of iterative reconvolution using the FluoFit. Fluorescence lifetime measurements between 1000 and 1600 nm were performed with an InGaAs photomultiplier tube module (H10330-75, Hamamatsu, Inc.). The output was fed into a digital oscilloscope (Tektronix TDS 520A) and averaged, which provides adequate temporal resolution of decay times in the microsecond range.

Solution Processed Solar Cells. *a. NiO Layer.* We followed the procedure of ref 27. Briefly, the nickel acetate tetrahydrate (Aldrich) was dissolved in methanol to a concentration of 0.4 M. An equimolar quantity of diethanolamine (Aldrich) was added under stirring. ITO substrate was cleaned by successive ultrasonic treatment in detergent, purified water, acetone, and propanol before drying under nitrogen. Thin films were prepared by spin-coating the sol−gel precursor onto the ITO substrate under ambient conditions at a spin speed of 3000 rpm for 30 s. Samples were then placed immediately into a tube furnace and annealed under air at 425 °C for 10 min, forming a dense, polycrystalline material. Film thicknesses were measured by a stylus profiler to be 30−40 nm thick.

b. ZnO Layers. ZnO nanoparticles were synthesized in ambient air. A 1.76 g portion of zinc acetate dihydrate was dissolved in 150 mL of ethanol with vigorous stirring and heated to 60 °C for 1 h. Parafilm was used to block solvent evaporation during the heating and the entire reaction time. In a separate container, 6.4 mL of a tetramethyl ammonium hydroxide (TMAH) solution (28% in MeOH) was added to 50 mL of ethanol. Over 10 min, the TMAH solution was slowly added to the zinc acetate solution at regular intervals. During this time the temperature of the zinc acetate solution was maintained at 60 °C with continuous stirring. Subsequently, the solution was heated at 60 °C for 30 min, after which the heater and stirrer were removed. After cooling to room temperature, the solution was kept refrigerated at ~5 °C. This mother-liquor solution was stable for over ~5 months. ZnO nanoparticles were collected from the refrigerated solution immediately before device fabrication. To prepare devices, 5 mL of the solution was typically mixed with 20 mL of hexane to precipitate the ZnO particles. After centrifugation, the supernatant was removed and the white precipitate was dissolved in isopropyl alcohol.

c. EDT-Treated PbS NC Layer Deposition. PbS NCs at 40 mg/mL in chlorobenzene were deposited by spin-coating from a Laurell WS-400A-6NPP-LITE. All spin steps were carried out at 1000 rpm for 30 s. First, 250 μL of NC solution was dispensed onto the substrate using an automatic pipet, and then the substrate was spun. Second, 1 mL of 0.1 M ethanedithiol in acetonitrile was swiftly dispensed on the substrate, left for 30 s, and then spun. The short EDT ligands replace the longer oleic acid ligands, improving conductivity through improved inter-NC coupling. Third, the substrate was rinsed with pure acetonitrile, spun, rinsed with pure chlorobenzene, and spun to remove residual ligand molecules and NCs. This three-step spin process of deposition, ligand exchange, and rinsing was one cycle. Three cycles were performed to produce ~100 nm thick NC films.

d. Fabrication of Solar Cells. The samples were loaded into a metal evaporator, and the evaporation chamber was pumped down to ultrahigh vacuum (~10^{-6} Torr). Au, Ag, or Al was thermally evaporated at a rate of 0.5 Å/sond for the first 100 Å and at 2−3 Å/sond for the rest of the deposition. Typically a total of 400−600 Å of metal electrode was deposited.

e. Device Characterization. Device testing was performed with a source measurement unit (Keithley 236). Samples were irradiated with 100 mW/cm^2 AM1.5 illumination from a Solar Light 16S-002 solar simulator. Light output power was calibrated with a Newport 818P-010-12 thermopile high-power detector. Small spectral mismatch was not taken into account in these measurements.

Room-Temperature Sputtered ZnO and NiO Layers. ZnO was deposited at a rate of 1.5 Å/s by reactively sputtering at a base pressure of 10^{-6} Torr with a 2 in. diameter Zn target in a 4:1 Ar/O_2 pressure ratio at 5 mTorr and 65 W of dc power. NiO was deposited at a rate of 1.7 Å/s by reactively sputtering at a base pressure of 10^{-6} Torr with a 2 in. diameter Ni target in a 99:1 Ar/O_2 pressure ratio at 10 mTorr and 57 W of dc power. Substrates sat on a rotating stage with a mask over the edges to keep the ITO bare for good electrical contact.

Conflict of Interest: The authors declare no competing financial interest.

Supporting Information Available: Transmission spectra, XRD patterns, AFM images of ZnO and NiO layers, and typical

transient fluorescence traces of PbS NCs in TCE and SiO_2−PbS NC−NiO composites are provided in the Supporting Information. This material is available free of charge *via* the Internet at http://pubs.acs.org.

Acknowledgment. Research was supported by the U.S. Department of Energy, Office of Basic Energy Sciences, Division of Materials Sciences and Engineering, under Award DE-SC0006647 (material synthesis and device fabrication) and an award (no. KUS-C1-018-02) made by King Abdullah University of Science and Technology (device testing). This work made use of the Cornell Center for Materials Research Shared Facilities, which are supported through the NSF MRSEC program (DMR-1120296).

REFERENCES AND NOTES

1. Choi, J. J.; Lim, Y.-F.; Santiago-Berrios, M. B.; Oh, M.; Hyun, B.-R.; Sun, L.; Bartnik, A. C.; Goedhart, A.; Malliaras, G. G.; Abruña, H. D.; *et al*. PbSe Nanocrystal Excitonic Solar Cells. *Nano Lett.* **2009**, *9*, 3749–3755.
2. Leschkies, K. S.; Beatty, T. J.; Kang, M. S.; Norris, D. J.; Aydil, E. S. Solar Cells Based on Junctions between Colloidal PbSe Nanocrystals and Thin ZnO Films. *ACS Nano* **2009**, *3*, 3638–3648.
3. Gao, J.; Luther, J. M.; Semonin, O. E.; Ellingson, R. J.; Nozik, A. J.; Beard, M. C. Quantum Dot Size Dependent J−V Characteristics in Heterojunction ZnO/PbS Quantum Dot Solar Cells. *Nano Lett.* **2011**, *11*, 1002–1008.
4. Pattantyus-Abraham, A. G.; Kramer, I. J.; Barkhouse, A. R.; Wang, X.; Konstantatos, G.; Debnath, R.; Levina, L.; Raabe, I.; Nazeeruddin, M. K.; Grätzel, M.; *et al*. Depleted-Heterojunction Colloidal Quantum Dot Solar Cells. *ACS Nano* **2010**, *4*, 3374–3380.
5. Kim, J. Y.; Kim, S. H.; Lee, H. H.; Lee, K.; Ma, W.; Gong, X.; Heeger, A. J. New Architecture for High-Efficiency Polymer Photovoltaic Cells Using Solution-Based Titanium Oxide as an Optical Spacer. *Adv. Mater.* **2006**, *18*, 572–576.
6. Park, S. H.; Roy, A.; Beaupre, S.; Cho, S.; Coates, N.; Moon, J. S.; Moses, D.; Leclerc, M.; Lee, K.; Heeger, A. J. Bulk Heterojunction Solar Cells with Internal Quantum Efficiency Approaching 100%. *Nat. Photonics* **2009**, *3*, 297–302.
7. Li, G.; Chu, C. W.; Shrotriya, V.; Huang, J.; Yang, Y. Efficient Inverted Polymer Solar Cells. *Appl. Phys. Lett.* **2006**, *88*, 253503–3.
8. White, M. S.; Olson, D. C.; Shaheen, S. E.; Kopidakis, N.; Ginley, D. S. Inverted Bulk-Heterojunction Organic Photovoltaic Device Using a Solution-Derived ZnO Underlayer. *Appl. Phys. Lett.* **2006**, *89*, 143517–3.
9. Waldauf, C.; Morana, M.; Denk, P.; Schilinsky, P.; Coakley, K.; Choulis, S. A.; Brabec, C. J. Highly Efficient Inverted Organic Photovoltaics Using Solution Based Titanium Oxide as Electron Selective Contact. *Appl. Phys. Lett.* **2006**, *89*, 233517–3.
10. Brown, P. R.; Lunt, R. R.; Zhao, N.; Osedach, T. P.; Wanger, D. D.; Chang, L.-Y.; Bawendi, M. G.; Bulović, V. Improved Current Extraction from ZnO/PbS Quantum Dot Heterojunction Photovoltaics Using a MoO_3 Interfacial Layer. *Nano Lett.* **2011**, *11*, 2955–2961.
11. Gao, J.; Perkins, C. L.; Luther, J. M.; Hanna, M. C.; Chen, H.-Y.; Semonin, O. E.; Nozik, A. J.; Ellingson, R. J.; Beard, M. C. n-Type Transition Metal Oxide as a Hole Extraction Layer in PbS Quantum Dot Solar Cells. *Nano Lett.* **2011**, *11*, 3263–3266.
12. Shrotriya, V.; Li, G.; Yao, Y.; Chu, C.-W.; Yang, Y. Transition Metal Oxides as the Buffer Layer for Polymer Photovoltaic Cells. *Appl. Phys. Lett.* **2006**, *88*, 073508.
13. Tao, C.; Ruan, S.; Xie, G.; Kong, X.; Shen, L.; Meng, F.; Liu, C.; Zhang, X.; Dong, W.; Chen, W. Role of Tungsten Oxide in Inverted Polymer Solar Cells. *Appl. Phys. Lett.* **2009**, *94*, 043311–3.
14. Mora-Sero, I.; Bertoluzzi, L.; Gonzalez-Pedro, V.; Gimenez, S.; Fabregat-Santiago, F.; Kemp, K. W.; Sargent, E. H.; Bisquert, J. Selective Contacts Drive Charge Extraction in Quantum Dot Solids *via* Asymmetry in Carrier Transfer Kinetics. *Nat. Commun.* **2013**, *4*, 2272.
15. Kim, D. Y.; Subbiah, J.; Sarasqueta, G.; So, F.; Ding, H.; Irfan; Gao, Y. The Effect of Molybdenum Oxide Interlayer on Organic Photovoltaic Cells. *Appl. Phys. Lett.* **2009**, *95*, 093304–3.
16. He, J.; Lindstrom, H.; Hagfeldt, A.; Lindquist, S.-E. Dye-Sensitized Nanostructured p-Type Nickel Oxide Film as a Photocathode for a Solar Cell. *J. Phys. Chem. B* **1999**, *103*, 8940–8943.
17. Gibson, E. A.; Smeigh, A. L.; Le Pleux, L.; Fortage, J.; Boschloo, G.; Blart, E.; Pellegrin, Y.; Odobel, F.; Hagfeldt, A.; Hammarström, L. A p-Type NiO-Based Dye-Sensitized Solar Cell with an Open-Circuit Voltage of 0.35 V. *Angew. Chem., Int. Ed.* **2009**, *48*, 4402–4405.
18. Li, L.; Gibson, E. A.; Qin, P.; Boschloo, G.; Gorlov, M.; Hagfeldt, A.; Sun, L. Double-Layered NiO Photocathodes for p-Type DSSCs with Record IPCE. *Adv. Mater.* **2010**, *22*, 1759–1762.
19. Nattestad, A.; Mozer, A. J.; Fischer, M. K. R.; Cheng, Y. B.; Mishra, A.; Bauerle, P.; Bach, U. Highly Efficient Photocathodes for Dye-Sensitized Tandem Solar Cells. *Nat. Mater.* **2010**, *9*, 31–35.
20. He, J. J.; Lindstrom, H.; Hagfeldt, A.; Lindquist, S. E. Dye-Sensitized Nanostructured Tandem Cell-First Demonstrated Cell with a Dye-Sensitized Photocathode. *Sol. Energy Mater. Sol. Cells* **2000**, *62*, 265–273.
21. Qin, P.; Zhu, H.; Edvinsson, T.; Boschloo, G.; Hagfeldt, A.; Sun, L. Design of an Organic Chromophore for P-Type Dye-Sensitized Solar Cells. *J. Am. Chem. Soc.* **2008**, *130*, 8570–8571.
22. Andrew, N.; Michael, F.; Robert, K.; Yi-Bing, C.; Udo, B. Dye-Sensitized Nickel(II)oxide Photocathodes for Tandem Solar Cell Applications. *Nanotechnology* **2008**, *19*, 295304.
23. Mori, S.; Fukuda, S.; Sumikura, S.; Takeda, Y.; Tamaki, Y.; Suzuki, E.; Abe, T. Charge-Transfer Processes in Dye-Sensitized NiO Solar Cells. *J. Phys. Chem. C* **2008**, *112*, 16134–16139.
24. Park, S.-Y.; Kim, H.-R.; Kang, Y.-J.; Kim, D.-H.; Kang, J.-W. Organic Solar Cells Employing Magnetron Sputtered p-Type Nickel Oxide Thin Film as the Anode Buffer Layer. *Sol. Energy Mater. Sol.* **2010**, *94*, 2332–2336.
25. Irwin, M. D.; Buchholz, D. B.; Hains, A. W.; Chang, R. P. H.; Marks, T. J. p-Type Semiconducting Nickel Oxide as an Efficiency-Enhancing Anode Interfacial Layer in Polymer Bulk-Heterojunction Solar Cells. *Proc. Natl. Acad. Sci. U.S.A.* **2008**, *105*, 2783–2787.
26. Caruge, J.-M.; Halpert, J. E.; Bulović, V.; Bawendi, M. G. NiO as an Inorganic Hole-Transporting Layer in Quantum-Dot Light-Emitting Devices. *Nano Lett.* **2006**, *6*, 2991–2994.
27. Mashford, B. S.; Nguyen, T. L.; Wilson, G. J.; Mulvaney, P. All-Inorganic Quantum-Dot Light-Emitting Devices Formed *via* Low-Cost, Wet-Chemical Processing. *J. Mater. Chem.* **2010**, *20*, 167–172.
28. Caruge, J. M.; Halpert, J. E.; Wood, V.; Bulovic, V.; Bawendi, M. G. Colloidal Quantum-Dot Llight-Emitting Diodes with Metal-Oxide Charge Transport Layers. *Nat. Photonics* **2008**, *2*, 247–250.
29. Powell, R. J.; Spicer, W. E. Optical Properties of NiO and CoO. *Phys. Rev. B* **1970**, *2*, 2182–2193.
30. Hüfner, S.; Steiner, P.; Sander, I.; Reinert, F.; Schmitt, H. The Optical Gap of NiO. *Z. Phys. B: Condens. Matter* **1992**, *86*, 207–215.
31. Kuiper, P.; Kruizinga, G.; Ghijsen, J.; Sawatzky, G. A.; Verweij, H. Character of Holes in Li_{x}Ni_{1-x}O and Their Magnetic Behavior. *Phys. Rev. Lett.* **1989**, *62*, 221–224.
32. Sawatzky, G. A.; Allen, J. W. Magnitude and Origin of the Band Gap in NiO. *Phys. Rev. Lett.* **1984**, *53*, 2339–2342.
33. Deng, R.; Yao, B.; Li, Y. F.; Zhao, Y. M.; Li, B. H.; Shan, C. X.; Zhang, Z. Z.; Zhao, D. X.; Zhang, J. Y.; Shen, D. Z.; *et al*. X-Ray Photoelectron Spectroscopy Measurement of n-ZnO/p-NiO Heterostructure Valence-Band Offset. *Appl. Phys. Lett.* **2009**, *94*, 022108.

34. Wood, V.; Panzer, M. J.; Halpert, J. E.; Caruge, J. M.; Bawendi, M. G.; Bulović, V. Selection of Metal Oxide Charge Transport Layers for Colloidal Quantum Dot LEDs. *ACS Nano* **2009**, *3*, 3581–3586.
35. Koffyberg, F. P.; Benko, F. A. p-Type NiO as a Photoelectrolysis Cathode. *J. Electrochem. Soc.* **1981**, *128*, 2476–2479.
36. Wu, H.; Wang, L.-S. A Study of Nickel Monoxide (NiO), Nickel Dioxide (ONiO), and Ni(O_2) Complex by Anion Photoelectron Spectroscopy. *J. Chem. Phys.* **1997**, *107*, 16–21.
37. Spear, W. E.; Tannhauser, D. S. Hole Transport in Pure NiO Crystals. *Phys. Rev. B* **1973**, *7*, 831.
38. Luther, J. M.; Law, M.; Beard, M. C.; Song, Q.; Reese, M. O.; Ellingson, R. J.; Nozik, A. J. Schottky Solar Cells Based on Colloidal Nanocrystal Films. *Nano Lett.* **2008**, *8*, 3488–3492.
39. Nair, G.; Chang, L.-Y.; Geyer, S. M.; Bawendi, M. G. Perspective on the Prospects of a Carrier Multiplication Nanocrystal Solar Cell. *Nano Lett.* **2011**, *11*, 2145–2151.
40. Ma, W.; Swisher, S. L.; Ewers, T.; Engel, J.; Ferry, V. E.; Atwater, H. A.; Alivisatos, A. P. Photovoltaic Performance of Ultrasmall PbSe Quantum Dots. *ACS Nano* **2011**, *5*, 8140–8147.
41. Maraghechi, P.; Labelle, A. J.; Kirmani, A. R.; Lan, X.; Adachi, M. M.; Thon, S. M.; Hoogland, S.; Lee, A.; Ning, Z.; Fischer, A.; *et al*. The Donor−Supply Electrode Enhances Performance in Colloidal Quantum Dot Solar Cells. *ACS Nano* **2013**, *7*, 6111–6116.
42. Yoon, W.; Boercker, J. E.; Lumb, M. P.; Placencia, D.; Foos, E. E.; Tischler, J. G. Enhanced Open-Circuit Voltage of PbS Nanocrystal Quantum Dot Solar Cells. *Sci. Rep.* **2013**, *3*, 2225.
43. Moormann, H.; Kohl, D.; Heiland, G. Work Function and Band Bending on Clean Cleaved Zinc Oxide Surfaces. *Surf. Sci.* **1979**, *80*, 261–264.
44. Zhao, S. Q.; Zhao, K.; Zhou, Q. L.; Zhou, Y. L.; Wang, S. F.; Ning, T. Y. Transient Infrared Laser-Induced Photovoltaic Effect of ZnO/MgB 2 Heterostructures. *J. Phys. D: Appl. Phys.* **2007**, *40*, 4489.
45. Aranovich, J. A.; Golmayo, D.; Fahrenbruch, A. L.; Bube, R. H. Photovoltaic Properties of ZnO/CdTe Heterojunctions Prepared by Spray Pyrolysis. *J. Appl. Phys.* **1980**, *51*, 4260–4268.
46. Hyun, B.-R.; Zhong, Y.-W.; Bartnik, A. C.; Sun, L.; Abruña, H. D.; Wise, F. W.; Goodreau, J. D.; Matthews, J. R.; Leslie, T. M.; Borrelli, N. F. Electron Injection from Colloidal PbS Quantum Dots into Titanium Dioxide Nanoparticles. *ACS Nano* **2008**, *2*, 2206–2212.
47. Luther, J. M.; Gao, J.; Lloyd, M. T.; Semonin, O. E.; Beard, M. C.; Nozik, A. J. Stability Assessment on a 3% Bilayer PbS/ZnO Quantum Dot Heterojunction Solar Cell. *Adv. Mater.* **2010**, *22*, 3704–3707.
48. Krüger, S.; Hickey, S. G.; Tscharntke, S.; Eychmüller, A. Study of the Attachment of Linker Molecules and Their Effects on the Charge Carrier Transfer at Lead Sulfide Nanoparticle Sensitized ZnO Substrates. *J. Phys. Chem. C* **2011**, *115*, 13047–13055.
49. Williams, R. Photoemission of Electrons from Silicon into Silicon Dioxide. *Phys. Rev.* **1965**, *140*, A569–A575.
50. Goodman, A. M.; John, J.; O'Neill, J. Photoemission of Electrons from Metals into Silicon Dioxide. *J. Appl. Phys.* **1966**, *37*, 3580–3583.
51. Laughlin, R. B. Optical Absorption Edge of SiO_2. *Phys. Rev. B* **1980**, *22*, 3021–3029.
52. Tvrdy, K.; Kamat, P. V. Substrate Driven Photochemistry of CdSe Quantum Dot Films: Charge Injection and Irreversible Transformations on Oxide Surfaces. *J. Phys. Chem. A* **2009**, *113*, 3765–3772.
53. Cánovas, E.; Moll, P.; Jensen, S. A.; Gao, Y.; Houtepen, A. J.; Siebbeles, L. D. A.; Kinge, S.; Bonn, M. Size-Dependent Electron Transfer from PbSe Quantum Dots to SnO_2 Monitored by Picosecond Terahertz Spectroscopy. *Nano Lett.* **2011**, *11*, 5234–5239.
54. Kongkanand, A.; Tvrdy, K.; Takechi, K.; Kuno, M.; Kamat, P. V. Quantum Dot Solar Cells. Tuning Photoresponse through Size and Shape Control of CdSe-TiO_2 Architecture. *J. Am. Chem. Soc.* **2008**, *130*, 4007–4015.
55. Marcus, R. A. On the Theory of Electron-Transfer Reactions. VI. Unified Treatment for Homogeneous and Electrode Reactions. *J. Chem. Phys.* **1965**, *43*, 679–701.
56. Marcus, R. A.; Sutin, N. Electron Transfers in Chemistry and Biology. *Biochim. Biophys. Acta, Rev. Bioenerg.* **1985**, *811*, 265–322.
57. Wood, A.; Giersig, M.; Hilgendorff, M.; Vilas-Campos, A.; Liz-Marzán, L. M.; Mulvaney, P. Size Effects in ZnO: The Cluster to Quantum Dot Transition. *Aust. J. Chem.* **2003**, *56*, 1051–1057.
58. Choi, J. J.; Wenger, W. N.; Hoffman, R. S.; Lim, Y.-F.; Luria, J.; Jasieniak, J.; Marohn, J. A.; Hanrath, T. Solution-Processed Nanocrystal Quantum Dot Tandem Solar Cells. *Adv. Mater.* **2011**, *23*, 3144–3148.
59. Talapin, D. V.; Murray, C. B. PbSe Nanocrystal Solids for n- and p-Channel Thin Film Field-Effect Transistors. *Science* **2005**, *310*, 86–89.
60. Luther, J. M.; Law, M.; Song, Q.; Perkins, C. L.; Beard, M. C.; Nozik, A. J. Structural, Optical, and Electrical Properties of Self-Assembled Films of PbSe Nanocrystals Treated with 1,2-Ethanedithiol. *ACS Nano* **2008**, *2*, 271–280.
61. Gao, J.; Jeong, S.; Lin, F.; Erslev, P. T.; Semonin, O. E.; Luther, J. M.; Beard, M. C. Improvement in Carrier Transport Properties by Mild Thermal Annealing of PbS Quantum Dot Solar Cells. *Appl. Phys. Lett.* **2013**, *102*, 043506.
62. Jean, J.; Chang, S.; Brown, P. R.; Cheng, J. J.; Rekemeyer, P. H.; Bawendi, M. G.; Gradečak, S.; Bulović, V. ZnO Nanowire Arrays for Enhanced Photocurrent in PbS Quantum Dot Solar Cells. *Adv. Mater.* **2013**, *25*, 2790–2796.
63. Wang, X.; Koleilat, G. I.; Fischer, A.; Tang, J.; Debnath, R.; Levina, L.; Sargent, E. H. Enhanced Open-Circuit Voltage in Visible Quantum Dot Photovoltaics by Engineering of Carrier-Collecting Electrodes. *ACS Appl. Mater. Interfaces* **2011**, *3*, 3792–3795.
64. Bhandari, K. P.; Roland, P. J.; Mahabaduge, H.; Haugen, N. O.; Grice, C. R.; Jeong, S.; Dykstra, T.; Gao, J.; Ellingson, R. J. Thin Film Solar Cells Based on the Heterojunction of Colloidal PbS Quantum Dots with CdS. *Sol. Energy Mater. Sol. Cells* **2013**, *117*, 476–482.
65. Loiudice, A.; Rizzo, A.; Grancini, G.; Biasiucci, M.; Belviso, M. R.; Corricelli, M.; Curri, M. L.; Striccoli, M.; Agostiano, A.; Cozzoli, P. D.; *et al*. Fabrication of Flexible All-Inorganic Nanocrystal Solar Cells by Room-Temperature Processing. *Energy Environ. Sci.* **2013**, *6*, 1565–1572.
66. Vandewal, K.; Tvingstedt, K.; Gadisa, A.; Inganas, O.; Manca, J. V. On the Origin of the Open-Circuit Voltage of Polymer-Fullerene Solar Cells. *Nat. Mater.* **2009**, *8*, 904–909.
67. Brabec, C. J.; Shaheen, S. E.; Winder, C.; Sariciftci, N. S.; Denk, P. Effect of LiF/Metal Electrodes on the Performance of Plastic Solar Cells. *Appl. Phys. Lett.* **2002**, *80*, 1288–1290.
68. Pettersson, L. A. A.; Roman, L. S.; Inganas, O. Modeling Photocurrent Action Spectra of Photovoltaic Devices Based on Organic Thin Films. *J. Appl. Phys.* **1999**, *86*, 487–496.
69. Law, M.; Beard, M. C.; Choi, S.; Luther, J. M.; Hanna, M. C.; Nozik, A. J. Determining the Internal Quantum Efficiency of PbSe Nanocrystal Solar Cells with the Aid of an Optical Model. *Nano Lett.* **2008**, *8*, 3904–3910.
70. Burkhard, G. F.; Hoke, E. T.; McGehee, M. D. Accounting for Interference, Scattering, and Electrode Absorption to Make Accurate Internal Quantum Efficiency Measurements in Organic and Other Thin Solar Cells. *Adv. Mater.* **2010**, *22*, 3293–3297.
71. Gilot, J.; Barbu, I.; Wienk, M. M.; Janssen, R. A. J. The Use of ZnO as Optical Spacer in Polymer Solar Cells: Theoretical and Experimental Study. *Appl. Phys. Lett.* **2007**, *91*, 113520–3.
72. Kawashima, T.; Ezure, T.; Okada, K.; Matsui, H.; Goto, K.; Tanabe, N. FTO/ITO Double-Layered Transparent Conductive Oxide for Dye-Sensitized Solar Cells. *J. Photochem. Photobiol., A* **2004**, *164*, 199–202.
73. Sato, H.; Minami, T.; Takata, S.; Yamada, T. Transparent Conducting p-type NiO Thin Films Prepared by Magnetron Sputtering. *Thin Solid Films* **1993**, *236*, 27–31.

74. Wang, X.; Koleilat, G. I.; Tang, J.; Liu, H.; Kramer, I. J.; Debnath, R.; Brzozowski, L.; Barkhouse, D. A. R.; Levina, L.; Hoogland, S.; *et al*. Tandem Colloidal Quantum Dot Solar Cells Employing a Graded Recombination Layer. *Nat. Photonics* **2011**, *5*, 480–484.
75. Ong, B. S.; Li, C.; Li, Y.; Wu, Y.; Loutfy, R. Stable, Solution-Processed, High-Mobility ZnO Thin-Film Transistors. *J. Am. Chem. Soc.* **2007**, *129*, 2750–2751.
76. Guziewicz, M.; Grochowski, J.; Borysiewicz, M.; Kaminska, E.; Domagala, J. Z.; Rzodkiewicz, W.; Witkowski, B. S.; Golaszewska, K.; Kruszka, R.; Ekielski, M.; *et al*. Electrical and Optical Properties of NiO Films Deposited by Magnetron Sputtering. *Opt. Appl.* **2011**, *41*, 431–440.
77. Hines, M. A.; Scholes, G. D. Colloidal PbS Nanocrystals with Size-Tunable Near-Infrared Emission: Observation of Post-Synthesis Self-Narrowing of the Particle Size Distribution. *Adv. Mater.* **2003**, *15*, 1844–1849.